Review

Chirality in microswimmer motion: From circle swimmers to active turbulence

Hartmut Löwen[a]

Institut für Theoretische Physik II: Weiche Materie, Heinrich-Heine Universität Düsseldorf, Universitätsstrasse 1, 40225 Düsseldorf, Germany

Abstract. In this minireview, recent progress in our understanding of the basic physical principles of microswimmers which perform a motion characterized by chirality is summarized. We discuss both the chiral motion of a single circle swimmer and the occurrence of bacterial turbulence where swirls of different chirality are formed spontaneously in an interacting ensemble of linear microswimmers. Some recent highlights in this context as obtained by theory, simulation and experiment are summarized and briefly discussed.

1 Introduction

The notion of chirality goes back to Lord Kelvin [1] who introduced it for the shape of bodies. Chirality of motion implies that handedness of the trajectories becomes important: for example, in two dimensions, clockwise motion is different from anticlockwise motion. This minireview briefly summarizes and reviews two aspects of chiral motion of *microswimmers*. Microswimmers are self-propelled objects that move at low Reynolds number in an embedding fluid. The swim mechanism of single swimmers and the collective behaviour of many swimmers which are governed by hydrodynamic and steric interactions are a hot research topic of the last years. As for recent reviews, we refer to [2–5]. Even a single self-propelled particle constitutes a system out of equilibrium such that new theoretical concepts as well as precise experimental measurements are needed to unravel the dynamical behaviour of swimmers. In principal there are two different types of swimmers: first of all, biology provides many examples for swimmers in the micro-domain like flagellated bacteria. Second, there artificial modelswimmers, mainly colloidal Janus particles, which can be exposed to fuel sources and self-propagate as well.

Microswimmers can possess a chiral shape (according to Lord Kelvin's notion). At low Reynolds numbers, this typically leads to a hydrodynamic coupling between translation and rotation motion [6–8]. This implies that a translated particle will simultaneously rotate which in most cases results in a helical trajectory [9–12] in three and a circular trajectory in two dimensions [13]. Therefore chirality or handedness in the particle shape will typically generate chirality in the motion.

---

[a] e-mail: `hlowen@hhu.de`

In this minireview, we shall discuss the dynamics of a chiral swimmer moving along circles. One important additional feature at the micron scale is the stochastic Brownian motion which smears out, on average, the directionality of the motion. We shall discuss the Brownian circle swimmer in detail and briefly mention some of its variants in various environments. Then we turn to chirality emerging as a collective effect as a new turbulent swirling state in dense self-propelled rod systems and bacterial suspensions. We intend to focus on the essential physics and describe recent developments and applications.

This minireview is organized as follows: In Sect. 2, we discuss a single circle swimmer while Sect. 3 is devoted to active or bacterial turbulence. We finish with some conclusions and an outlook in Sect. 4.

2 Chirality in circle swimming

2.1 Active Brownian motion with chirality (circle swimming)

Swimming along a straight line (corresponding to linearly directed Brownian motion) is the exception rather than the rule. Ideal straight swimming only occurs if the left-right symmetry relative to the internal propulsion direction is not broken. A linear trajectory is getting unstable with respect to small deviations from this symmetry exhibiting a *chirality*. In two spatial dimensions, this will result in circle-swimming, in three dimensions, correspondingly, there is swimming along a helical path ("helical swimming"). Clearly one can assign a chirality (or helicity) to the path, the sign of which determines whether the motion is clockwise or anti-clockwise.

The occurence of spiral-like swimming motions of microorganisms was pointed out more than a century ago by Jennings [14] and since then was found in many different situations, in particular close to a substrate where certain bacteria [15–20] and spermatozoa [21–23] swim in circles. Likewise helical motion was observed for different bacteria and sperm cells [12,14,24–31]. Examples for non-living but active particles moving in circles are spherical camphors at an air–water interface [32] and chiral colloidal swimmers on a substrate [33,34]. The latter have provided excellent model systems to test the basic assumptions of chiral active Brownian motion. Finally, trajectories of deformable active particles [35] and even of completely blinded and ear-plugged pedestrians [36,37] can possess significant circular characteristics.

The origin of chiral motion can be manifold. The most obvious is an anisotropy in the particle shape which leads to a translation-rotation coupling in the hydrodynamic sense [6]. But also an anisotropy in the propulsion mechanism itself generates chiral motion. An example where both mechanisms are simultaneously at work is presented in Fig. 1. Here trajectories of two L-shape swimmers with different chiralities are shown. A cluster of linear swimmers which sticks together by direct forces [38] or by hydrodynamics or just by the activity itself [39] will in general lead to a situation where the total torque acting on the cluster center is not vanishing [40]. This leads to circling clusters. Finally the particle rotation can be induced by external fields, a standard example is a magnetic field perpendicular to the plane of motion which will exert a torque on the particles [41,42].

The equations of motion for chiral swimming can easily be understood in two spatial dimensions. Consider a polar particle as described by a center-of-mass coordinate $\mathbf{r}$ and a unit orientation vector $\hat{\mathbf{u}}$ which has a relative orientation with respect to the x-axis as given by the angle ϕ such that $\hat{\mathbf{u}} = (\cos\phi, \sin\phi)$, see Fig. 2 for a schematic illustration. We consider overdamped Brownian motion for both transla-tional and orientational degrees of freedom and introduce a systematic drift in the
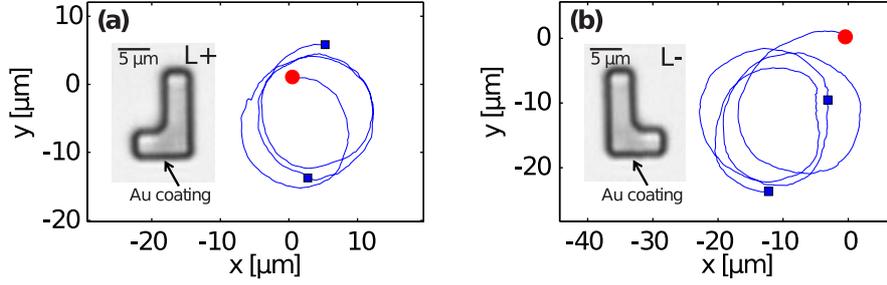
Fig. 1. Trajectories of an (a) L^+ and (b) L^- swimmer driven by self-diffusiophoresis. (Red) bullets and (blue) square symbols correspond to initial particle positions and those after 1 min each, respectively. The insets show microscope images of two different swimmers with the Au coating (not visible in the bright-field image) indicated by an arrow. From Ref. [33].
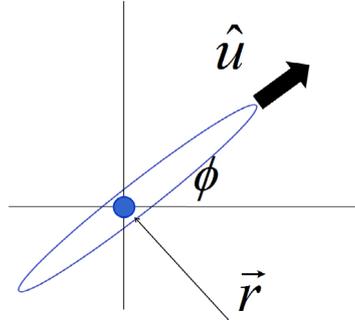

Fig. 2. Sketch of the orientation $\hat{\mathbf{u}}$ and position $\mathbf{r}$ of an active rod.

orientation as mediated by a constant torque M in the direction perpendicular to the plane of motion. The equations of motion therefore are

$$\dot{\mathbf{r}} = \beta \overset{\leftrightarrow}{D} \left(F\hat{\mathbf{u}} - \boldsymbol{\nabla} V\left(\mathbf{r}, \phi\right) + \mathbf{f}\right) \tag{1}$$

$$\dot{\phi} = \beta D_r \left(M - \partial_\phi V\left(\mathbf{r}, \phi\right) + \tau\right). \tag{2}$$

Here, $V(\mathbf{r}, \phi)$ is an external one-body potential that can be set to zero, $\mathbf{f}$ and τ are Gaussian distributed random numbers characterizing the Brownian noise for the translation and rotation. While their first moment is vanishing, their second moment is related to an (effective) system temperature T (with $\beta = 1/k_B T$).

Finally F is an effective self-propulsion force directed along the particle orientation which is proportional to the swimming speed. The term βD_r is an inverse rotational friction coefficient such that D_r is the rotational diffusion coefficient. The translational diffusion tensor is given by

$$\overset{\leftrightarrow}{D} = D_\parallel \hat{\mathbf{u}} \otimes \hat{\mathbf{u}} + D_\perp \left(\overset{\leftrightarrow}{I} - \hat{\mathbf{u}} \otimes \hat{\mathbf{u}}\right) \tag{3}$$

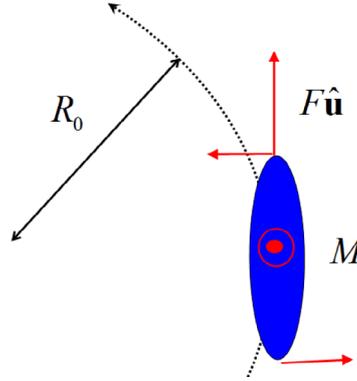with two translational diffusion constants perpendicular and parallel to the orientation.

Fig. 3. Trajectory of a circle swimmer and direction of the self-propulsion force $F\hat{\mathbf{u}}$ and torque M.
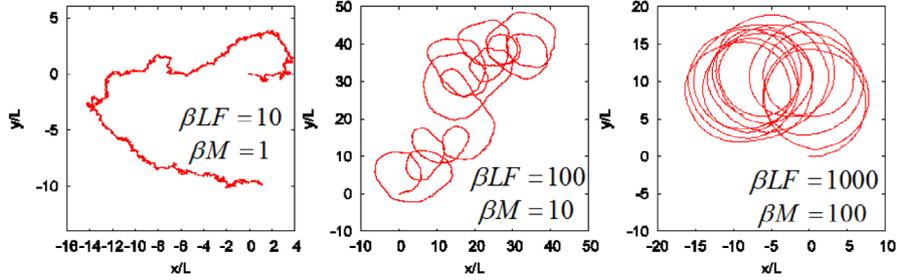

Fig. 4. Typical Brownian dynamics simulation results for the trajectory of a circle swimmer. The different snapshots are for three different noise strengths.

Let us discuss the solution of these equations in the bulk when $V(\mathbf{r}, \phi)$ is vanishing. In the noise free case ($\mathbf{f} = 0$ and $\tau = 0$) the deterministic solution of the equations of motion (1) and (2) are closed circles, see Fig. 3. The circle radius is given by

$$R_0 = \frac{D_\parallel F}{D_r M} \tag{4}$$

and the spinning frequency ω is

$$\omega = \beta D_r M. \tag{5}$$

For finite noise, there are three regimes: for very short times the motion is diffusive, then there is a crossover towards a (albeit curved) ballistic regime and then for very long times there is again diffusion. Examples for circle-swimming particle trajectories are presented in Fig. 4 at three different strengths of noise. The first two noise-average moments of the circle swimmer can be computed analytically [43] generalizing the seminal result of Howse et al for linear swimmers [44]. One obtains

$$\overline{\mathbf{r} - \mathbf{r}(0)} = \lambda \left[D_r \hat{\mathbf{u}}_0^\perp - e^{-D_r t} \left(D_r \bar{\hat{\mathbf{u}}} + \omega \bar{\hat{\mathbf{u}}}^\perp \right) \right] \tag{6}$$

$$\overline{(\mathbf{r} - \mathbf{r}(0))^2} = 2\lambda^2 \Big\{ \omega^2 - D_r^2 + D_r \left(D_r^2 + \omega^2 \right) t$$
$$+ e^{-D_r t} \left[\left(D_r^2 - \omega^2 \right) \cos(\omega t) - 2 D_r \omega \sin(\omega t) \right] \Big\} + 2 \left(D_\parallel + D_\perp \right) t \tag{7}$$

where the overbar denotes a noise-average, λ is defined as

$$\lambda = \beta D_\parallel F / \left(D_r^2 + \omega^2 \right) \tag{8}$$

$\hat{\mathbf{u}}(0) = (\cos\phi_0, \sin\phi_0)$ is the initial orientation and $\mathbf{r}(0)$ the initial position. Moreover

$$\hat{\mathbf{u}}_{\mathbf{0}}^{\perp} = (-\sin\phi_0, \; \cos\phi_0) \tag{9}$$

$$\overline{\hat{\mathbf{u}}} = \left(\cos\bar{\phi}, \; \sin\bar{\phi}\right) \tag{10}$$

$$\overline{\hat{\mathbf{u}}^{\perp}} = \left(-\sin\bar{\phi}, \; \cos\bar{\phi}\right) \tag{11}$$

where $\bar{\phi}$ is the noise average over the angles given by

$$\bar{\phi} = \phi_0 + \omega t. \tag{12}$$

For a linear swimmer, the first moment simplifies to

$$\overline{\mathbf{r}(t)} = \mathbf{r}(0) + \hat{\mathbf{u}}(0)\frac{v_0}{D_r}(1 - \exp(-D_r t)) \tag{13}$$

where $v_0 = \beta D_{\parallel} F$ is the self-propulsion speed. So for given initial position and orientation it is a piece of a straight line directed along the initial orientation. Interestingly the swimmer on average does not proceed to infinity but only recovers a characteristic persistence length which is given by $\ell_p = v_0/D_r$.

Discussing the first moment (6) for chiral swimmers is more complicated. The mean trajectory is now generalized to a *spira mirabilis* or a logarithmic spiral. This logarithmic spiral was first introduced by Descartes and then studied by Jacob Bernoulli. By eliminating the time t, one obtains the following representation for the trajectory in polar coordinates

$$r(\phi) \propto \exp(-D_r(\phi - \phi_0)/\omega) \tag{14}$$

where ω is the characteristic circling frequency. Recent experiments on chiral colloidal microswimmers have confirmed this prediction [33] as documented in Fig. 5. Moreover, a general and elegant matrix technique was proposed to solve the stochastic equations of motion efficiently [45].

Finally, in three dimensions, the noise-averaged trajectory is a concho-spiral [46] which is the appropriate generalization of the logarithmic spiral.

2.2 Circle swimmers in gravity

The motion of circle swimmer in an external gravitational field has been studied by experiments and theory by using L-shaped artificial swimmers on a tilted two-dimensional substrate. Interestingly a situation of negative gravitaxis was found where the chiral self-propelled particles swim against gravity [47]. The physical origin is a balance of torques which arise from the self-propulsion and from gravity. The resulting motion is linear. This mechanism does only occur for chiral anisotropic particles and is different from bottom-heaviness [48] which is another reason for negative gravitaxis.

2.3 Circle swimmers in other environments

Circle swimmers were considered and studied in various external fields (for linear swimmers in external fields see [49]). In linear channels, the compensation of the inner torque with a torque exerted externally by the wall can lead to a stable sliding mode of circle swimmers along the channel wall [43,50]. For more aspects of swimmers
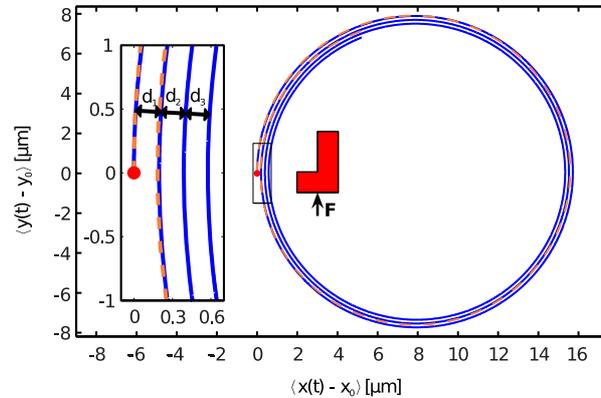
Fig. 5. Noise-averaged trajectory of a Brownian circle swimmer for a prescribed position and orientation at $t = 0$. The dashed curve is the experimental one obtained for a chiral L-shaped colloidal model swimmer. The solid curve shows the theoretical prediction of the *spira mirabilis* with the starting point indicated by a red bullet. Inset: close-up of the framed area in the plot. As a characteristic feature of the logarithmic spiral, the ratio d_{i+1}/d_i of the distances d_i between adjacent turns of the mean swimming path are constant. From Ref. [33].

near walls see [51]. Moreover circle swimmers in sinoidal walls [52], in periodic external potentials [53] and in asymmetrically patterned arrays [54] have been addressed in order to steer and optimize their directed motion. A trap device was proposed to catch swimmers with a certain chirality while releasing swimmers with an opposite chirality [55] such that it acts as a sorting device [56]. A similar separation was found in mixtures of circle swimmers with different chiralities in periodically structured walls [57]. Finally a circle swimmer with periodic time-dependent self-propulsion leads to self-similar first moments [58] generalizing the spira mirabilis result which occurs at constant propulsion.

3 Bacterial turbulence

3.1 The bulk state of active turbulence

Particle-resolved simulations of active rods have given valuable hints for bacterial turbulence, for more aspects of active rods see [59]. Based on a self-propelled rod model of linear swimmers, the emerging bulk state diagram was explored by Wensink and coworkers [60,61] as a function of two parameters, namely the area fraction ϕ and the aspect ratio of the rods. The temperature was set to zero and the strength of the self-propelling force relative to the repulsive interaction was kept fixed. The simulations were performed in two spatial dimensions. In the two-dimensional parameter space, a rich state diagram was found which is shown in Fig. 6.

For small densities, obviously a dilute phase is found which lacks any significant swarming. For higher densities and large aspect ratios, a swarming state occurs where large clusters are formed by aligning interactions and self-propulsion. This swarming state shows the characteristics of large density fluctuations and is therefore different to mobility-induced phase separation [62,63]. For small aspect ratios, on the other hand, there is a jammed state at high densities. Exactly at aspect ratio of 1 (spherical particles) an active crystal is formed [64,65]. For both high density and high aspect ratio, a lane phase occurs as in driven passive systems [66,67]. Interesting and novel
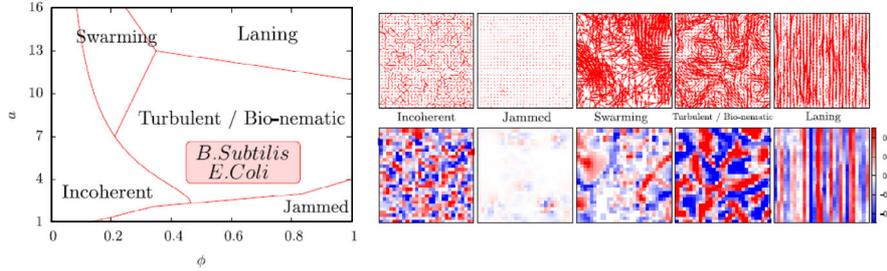
Fig. 6. Schematic non-equilibrium phase diagram of the 2D self-propelled rod model at variable aspect ratio a and effective density ϕ. The area relevant to self-motile bacteria is highlighted in red. A number of distinctly different dynamical states are discernible as indicated by the coarse-grained maps of the velocity field $v(\mathbf{r}, t)$ (upper panels) at time t and the corresponding scalar vorticity field $\tilde{\omega}(\mathbf{r}, t) = [\nabla \times v(\mathbf{r}, t)] \cdot \hat{e}_z$ expressed in units of τ_0^{-1}. Here, $\tau_0 = \lambda f_0 / F$ is a characteristic time scale composed of the self-propelling force F, the Stokes friction coefficient f_0 of a single bead and the steric interaction range λ. From Ref. [61].

behaviour is visible for intermediate parameters: there is a bionematic and a "turbulent" state. The former state is mainly characterized by nematic ordering while the latter possesses a significant degree of swirling. Though a bit arbitrary, the distinction between bionematic and turbulent state can be done via the behaviour of the equal-time autocorrelation function of the coarse-grained velocity field $v(\mathbf{r}, t)$ as a function of distance r: If it crosses zero at a certain distance $r = R$ this marks the radius R of a typical swirl and the state is called "turbulent" if it does not cross zero, it is called "bionematic". Such a velocity correlation function is shown in Fig. 8.

The turbulent state occurs at aspect ratios which are typical for real bacteria such as E. coli or bacillus subtilis. Indeed experiments on strongly confined bacteria have confirmed the occurence of a turbulent state. The enstrophy Ω of a coarse-grained velocity field of the swimmers is another more sensible order parameter for the "turbulent" state. It is defined as

$$\Omega = \frac{1}{2} \langle |\widetilde{\omega}(\mathbf{r}, t)|^2 \rangle \tag{15}$$

with $\omega(\mathbf{r}, t) = [\nabla \times v(\mathbf{r}, t)] \cdot \hat{e}_z$ and the tilde means a spatial average. In the turbulent state, the averaged chirality is zero. Still there is a significant local chirality as revealed by the strong peaks in the vorticity of the coarse-grained velocity field, see Fig. 6. A significant degree of swirling is visible there. There is also a characteristic extension of the swirls which is about 30 larger than the size of the self-propelled rods. Moreover in Fig. 7 experimental data for bacillus subtilis suspensions in the turbulent state and results from an extension of the Toner-Tu model of active nematics which includes a gradient expansion and is performed in the incompressible limit are shown. More details about the theory can be found in Refs. [60, 68]. An alternate approach to active turbulence has recently been established using a mean-field theory of active nematics for an incompressible flow [69]. Finally, active turbulence was also found in models which enforce alignment at small particle separation and anti-alignment for larger distances [70]. Then the crossover distance sets the swirl size.

It is important to note that in many occasions the term turbulence is reserved for fluid motion at high Reynolds number complementary to the present situation which happens at low Reynolds number. However, the Greek work "$\tau\upsilon\rho\beta\eta$" from which the word turbulence roots means perturbation or swirling in a quite general sense. Therefore the term "turbulence" can be used in a more general way. In order
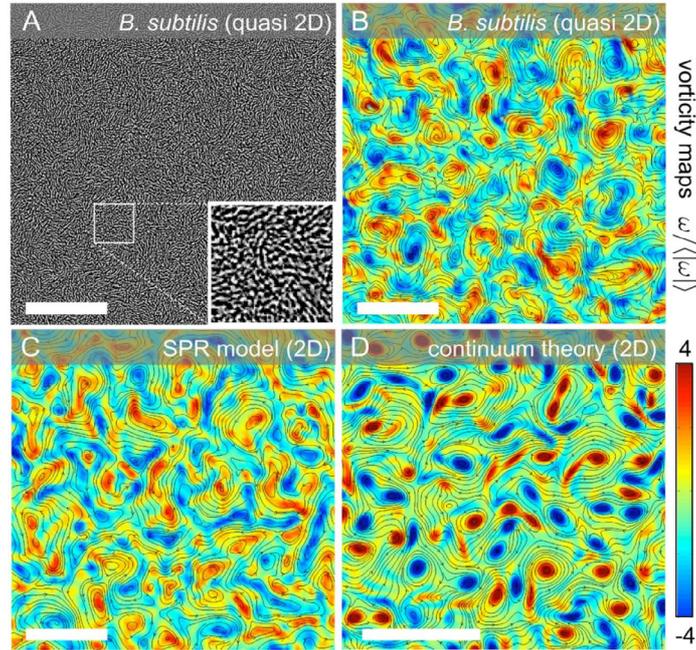
Fig. 7. Experimental snapshot (A) of a highly concentrated, homogeneous quasi-2D bacterial suspension. Flow streamlines $\mathrm{v}(t,\mathbf{r})$ and vorticity fields $\omega(t,\mathbf{r})$ in the turbulent regime, as obtained from (B) quasi-2D bacteria experiments, (C) simulations of the deterministic self-propelled rod model ($a = 5$; $\phi = 0.84$), and (D) continuum theory. The range of the simulation data in D was adapted to the experimental field of view ($217\,\mu\mathrm{m} \times 217\,\mu\mathrm{m}$) by matching the typical vortex size (Scale bars, $50\,\mu\mathrm{m}$). From Ref. [60].

to avoid confusion, the term "active turbulence" [71] or "**bacterial turbulence**" [68] has been introduced which delineates the effect considered here from high-Reynolds number turbulence. Another term which has been used is "mesoscale turbulence" [60] which stresses the fact that there is a maximal swirl size which is also different to traditional turbulence where swirls occur on all scales.

Finally the scaling of the energy spectrum has been explored as well. An interesting question is whether the traditional Kolmogorow-Kraichnan scaling of high-Reynolds-number turbulence is valid. This would be a power-law decay in the inertial regime where the energy spectrum

$$E(k) \sim k \int d\mathbf{r}\, \exp[i\mathbf{k} \cdot \mathbf{r}] \langle \mathrm{v}(t,0) \cdot \mathrm{v}(t,\mathbf{r}) \rangle_t \qquad (16)$$

scales with the wave number k as $k^{-5/3}$. In fact this exponent is not found in bacterial turbulence (see Fig. 8) where rather an exponent $-8/3$ shows up in the limited scaling window. Therefore bacterial turbulence is qualitatively different from ordinary turbulence at high Reynolds numbers. It is still unclear since the scaling regime is limited by the typical inverse swirl size whether the found exponent is universal or whether it is nonuniversal or just a crossover. More evidence for a true scaling has been obtained in the opposite limit of small wave numbers k. Here recent studies [72] have found that there is another scaling limit characterized by a nonuniversal exponent which can be in general different to the one occuring in the Kolmogorov-Kraichnan scaling. This nicely demonstrates that bacterial turbulence is a complex phenomenon which lacks universal scaling.
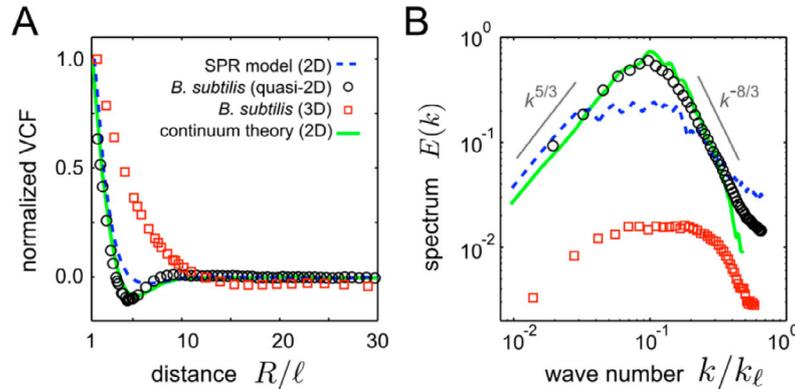
Fig. 8. Equal-time velocity correlation functions (VCFs), normalized to unity at $R = \ell$, and flow spectra for the two-dimensional self-propelled-rod model, B. subtilis experiments, and 2D continuum theory. (A) The minima of the VCFs reflect the characteristic vortex size R_v. Data points present averages over all directions and time steps to maximize sample size. (B) For bulk turbulence (red squares) the 3D spectrum is plotted ($k_\ell = 2\pi/\ell$), the other curves show 2D spectra. Spectra for the 2D continuum theory and quasi-2D experimental data are in good agreement; those of the 2D SPR model and the 3D bacterial data show similar asymptotic scaling but exhibit an intermediate plateau region (spectra multiplied by constants for better visibility and comparison). From Ref. [60].

3.2 What can we do with bacterial turbulence?

After we have clarified the occurence of bacterial turbulence in the bulk (in two spatial dimensions), we now turn to the effect of boundaries of bacterial turbulence. The understanding of this leads to important applications such as the motion of passive objects in a turbulent bath. An important feature found in Ref. [73] is that a hard boundary just suppresses the occurence of swirls. This leads directly to a depletion of swirls in a cuspy environment which has important consequences.

a) Single carrier
   A standard example of a nontrivial nonlinear geometry is a wedge-like carrier (a V-shaped passive particle). Let us assume that the size of the carrier is comparable to the typical swirl size R. Then there is an important difference between the inside and the outside region of the carrier as far as the occurence of swirls is concerned which is illustrated in Fig. 9.

   The outside does not put any constraint for a full swirl while the inside when narrow enough excludes full swirls. Hence we expect a depletion of swirls inside close to the cusp which results in an area shielded from swirks. This is in fact confirmed by computer simulation of the self-propelled rod model. The swirl depletion induces a translational motion of the carrier along its cusp. At the inner wedge cusp, rods are accumulating which are pushing the carrier. As these are shielded from swirls, they provide an efficient and powerful driving source of the carrier such that the bacterial-induced velocity of the carrier is optimized in the turbulent bulk phase of the rods.

b) Two carriers
   When an active bath is exposed to two carriers fixed in their relative orientation, swirl depletion again plays the key role in driving their joint motion. There is a depletion attraction between neighbouring rods driving them together and ultimately leading to stacking of the carriers. This is demonstrated in Fig. 10.
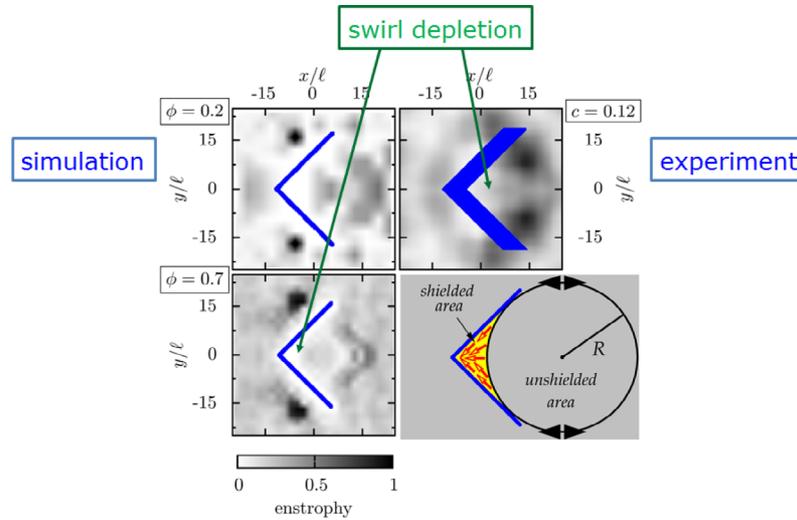
Fig. 9. Normalized local magnitude of vorticity obtained from simulations (left column) and experiment (top right). Bottom right: Illustration of swirl shielding in the carrier cusp. Bacteria in the shielded area (light colored) are indicated by arrows and the unshielded area is marked by dark color. The typical swirl radius R for different bacteria concentrations is obtained as the first minimum of the equal-time spatial velocity autocorrelation function. From Ref. [73].
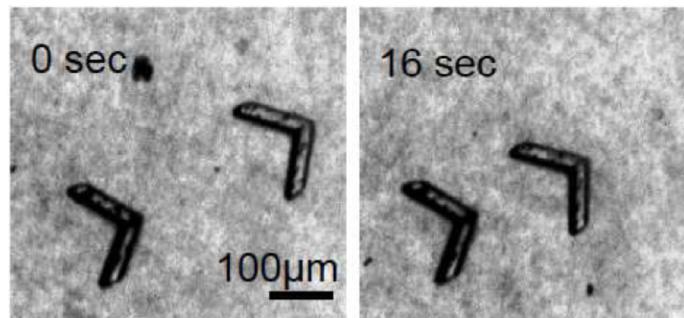

Fig. 10. Illustration of the attraction of wedge-like carriers in a turbulent bacterial bath. The two wedges approach each other as a function of time. From Ref. [74].

Of course, many carriers are expected to pile up in long stacks similar to the behaviour of colloidal bowls [75].

c) Other effects

The occurence of bacterial turbulence was explored in the presence of many passive particles which were strongly interacting thus forming a stable network with a tunable spacing. Experiments and computer simulations [76,77] have shown that turbulence is suppressed if the characteristic spacing between the passive particles becomes comparable to the swirl size. This demonstrates that bacterial turbulence can be tailored at wish by using passive particles as obstacles and gives a first insight about bacterial turbulence in heterogeneous media (such as porous materials).

For mobile and weakly interacting passive particles, on the other hand, one can expect on the grounds of swirl depletion that a phase separation between the

passive particles occurs as induced by turbulence. However, the precise conditions for phase separation still need to be elaborated.

Recently bacterial turbulence was used in a complicated array system with some fascinating analogy to a binary Ising spin system [78]. Therefore turbulence might be possibly used for encoding information.

4 Conclusions and outlook

We have considered recent aspects of chiral circling motion of microswimmers. First we studied active Brownian motion of a single circle swimmer. In this case the circular motion is induced by an intrinsic left-right asymmetry of the swimmer. Then we have considered the collective motion of linear swimmers where large swirls are emerging due to excluded volume interactions and self-propulsion.

While single circle swimmers are well understood by now there is a number of future problems which will be explored soon in this rapidly developing field. We are just at the beginning to understand the collective behaviour of many circle swimmers [79,80] which may form vortex pairs. Moreover the universality or non-universality of bacterial turbulence needs to be explored more extending recent ideas [72]. It would be interesting to confirm a turbulent state also in suspensions of rod-like artificial microswimmers and to construct a microscopic theory for this new class of turbulence. Finally microswimmer motion can occur also on a nonplanar manifold [81]. It would be interesting to check the occurence of turbulence on a sphere of finite radius where the swirl size competes with the sphere diameter.

References

1. S.W.T.L. Kelvin, *The Molecular Tactics of a Crystal* (Clarendon Press, 1894)
2. P. Romanczuk, M. Bär, W. Ebeling, B. Lindner, L. Schimansky-Geier, Eur. Phys. J. Special Topics **202**, 1 (2012)
3. J. Elgeti, R.G. Winkler, G. Gompper, Rep. Prog. Phys. **78**, 056601 (2015)
4. A.M. Menzel, Physics Reports **554**, 1 (2015)
5. C. Bechinger, R. di Leonardo, H. Löwen, C. Reichhardt, G. Volpe, accepted in Rev. Mod. Phys. (2016) [`arXiv:1602.00081`]
6. D.J. Kraft, R. Wittkowski, B. ten Hagen, K.V. Edmond, D.J. Pine, H. Löwen, Phys. Rev. E **88**, 050301(R) (2013)
7. E.E. Keaveny, S.W. Walker, M.J. Shelley, Nano Lett. **13**, 531 (2013)
8. E.E. Keaveny, M.J. Shelley, Phys. Rev. E **79**, 051405 (2009)
9. A. Ghosh, P. Fischer, Nano Lett. **9**, 2243 (2009)
10. B.M. Friedrich, F. Jülicher, Phys. Rev. Lett. **103**, 068102 (2009)
11. S. Namdeo, S.N. Khaderi, P.R. Onck, Proc. R. Soc. A **470**, 20130547 (2014)
12. T.-W. Su, I. Choi, J. Feng, K. Huang, E. McLeod, A. Ozcan, Scientific Reports **3**, 1664 (2013)
13. R. Ledesma-Aguilar, H. Löwen, J.M. Yeomans, Eur. Phys. J. E **35**, 70 (2012)
14. H.S. Jennings, Am. Soc. Natural. **35**, 369 (1901)
15. H.C. Berg, L. Turner, Biophys. J. **58**, 919 (1990)
16. W.R. DiLuzio, L. Turner, M. Mayer, P. Garstecki, D.B. Weibel, H.C. Berg, G.M. Whitesides, Nature **435**, 12714 (2005)
17. E. Lauga, W.R. DiLuzio, G.M. Whitesides, H.A. Stone, Biophys. J. **90**, 400 (2006)
18. J. Hill, O. Kalkanci, J.L. McMurry, H. Koser, Phys. Rev. Lett. **98**, 068101 (2007)
19. V.B. Shenoy, D.T. Tambe, A. Prasad, J.A. Theriot, PNAS **104**, 8229 (2007)
20. S. Schmidt, J. van der Gucht, P.M. Biesheuvel, R. Weinkamer, E. Helfer, A. Fery, Eur. Biophys. J. **37**, 1361 (2008)

21. I.H. Riedel, K. Kruse, J. Howard, Science **309**, 300 (2005)
22. D.M. Woolley, Reproduction **126**, 259 (2003)
23. B.M. Friedrich, F. Jülicher, New J. Phys. **10**, 123025 (2008)
24. G. Corkidi, B. Taboada, C.D. Wood, A. Guerrero, A. Darszon, Biochem. Biophys. Res. Commun. **373**, 125 (2008)
25. C.J. Brokaw, J. Exp. Biol. **35**, 192 (1958)
26. C.J. Brokaw, J. Cell. Comp. Physiol. **54**, 95 (1959)
27. H.C. Crenshaw, American Zoologist **36**, 608 (1996)
28. T. Fenchel, N. Blackburn, Protist **150**, 325 (1999)
29. M.J. McHenry, J.A. Strother, Marine Biology **142**, 173 (2003)
30. G. Jékely, J. Colombelli, H. Hausen, K. Guy, E. Stelzer, F. Nédélec, D. Arendt, Nature **456**, 395 (2008)
31. R. Thar, T. Fenchel, Appl. Environ. Microbiol. **67**, 3299 (2001)
32. S. Nakata, Y. Iguchi, S. Ose, M. Kuboyama, T. Ishii, K. Yoshikawa, Langmuir **13**, 4454 (1997)
33. F. Kümmel, B. ten Hagen, R. Wittkowski, I. Buttinoni, R. Eichhorn, G. Volpe, H. Löwen, C. Bechinger, Phys. Rev. Lett. **110**, 198302 (2013)
34. M.S.D. Wykes, J. Palacci, T. Adachi, L. Ristroph, X. Zhong, M.D. Ward, J. Zhang, M.J. Shelley, Soft Matter **12**, 4584 (2016)
35. T. Ohta, T. Ohkuma, Phys. Rev. Lett. **102**, 154101 (2009)
36. T. Obata, T. Shimizu, H. Osaki, H. Oshima, H. Hara, J. Korean Phys. Soc. **46**, 713 (2005)
37. J.L. Souman, I. Frissen, M.N. Sreenivasa, M.O. Ernst, Curr. Biol. **19**, 1538 (2009)
38. G.S. Redner, A. Baskaran, M.F. Hagan, Phys. Rev. E **88**, 012305 (2013)
39. I. Buttinoni, J. Bialke, F. Kümmel, H. Löwen, C. Bechinger, T. Speck, Phys. Rev. Lett. **110**, 238301 (2013)
40. A. Kaiser, K. Popowa, H. Löwen, Phys. Rev. E. **92**, 012301 (2015)
41. A. Cēbers, J. Magn. Magn. Mater. **323**, 279 (2011)
42. W. Schirmacher, B. Fuchs, F. Höfling, T. Franosch, Phys. Rev. Lett. **115**, 240602 (2015)
43. S. van Teeffelen, H. Löwen, Phys. Rev. E **78**, 020101(R) (2008)
44. J.R. Howse, R.A.L. Jones, A.J. Ryan, T. Gough, R. Vafabakhsh, R. Golestanian, Phys. Rev. Lett. **99**, 048102 (2007)
45. A. Nourhani, P.E. Lammert, A. Borhan, V.H. Crespi, Phys. Rev. E **89**, 062304 (2014)
46. R. Wittkowski, H. Löwen, Phys. Rev. E **85**, 021406 (2012)
47. B. ten Hagen, F. Kümmel, R. Wittkowski, D. Takagi, H. Löwen, C. Bechinger, Nat. Commun. **5**, 4829 (2014)
48. K. Wolff, A.M. Hahn, H. Stark, Eur. Phys. J. E **36**, 43 (2013)
49. H. Stark, Eur. Phys. J. Special Topics **225**, 3069 (2016)
50. P.K. Radtke, L. Schimansky-Geier, Phys. Rev. E **85**, 051110 (2012)
51. J. Elgeti, G. Gompper, Eur. Phys. J. Special Topics **225**, 3033 (2016)
52. X. Ao, P.K. Ghosh, Y. Li, G. Schmid, P. Hänggi, F. Marchesoni, EPL **109**, 10003 (2015)
53. A. Nourhani, V.H. Crespi, P.E. Lammert, Phys. Rev. Lett. **115**, 118101 (2015)
54. C. Reichhardt, C.J.O. Reichhardt, Phys. Rev. E **88**, 042306 (2013)
55. M. Mijalkov, G. Volpe, Soft Matter **9**, 6376 (2013)
56. Q. Chen, B. Ai, J. Chem. Phys. **143**, 104113 (2015)
57. B. Ai, Y. He, W. Zhong, Soft Matter **11**, 3852 (2015)
58. S. Babel, B. ten Hagen, H. Löwen, J. Stat. Mech. **2014**, P02011 (2014)
59. F. Peruani, Eur. Phys. J. Special Topics **225**, 3001 (2016)
60. H.H. Wensink, J. Dunkel, S. Heidenreich, K. Drescher, R.E. Goldstein, H. Löwen, J.M. Yeomans, PNAS **109**, 14308 (2012)
61. H.H. Wensink, H. Löwen, J. Phys.: Condens. Matter **24**, 464130 (2012)
62. T. Speck, Eur. Phys. J. Special Topics **225**, 2287 (2016)
63. D. Marenduzzo, Eur. Phys. J. Special Topics **225**, 2065 (2016)
64. J. Bialké, T. Speck, H. Löwen, Phys. Rev. Lett. **108**, 168301 (2012)
65. A.M. Menzel, H. Löwen, Phys. Rev. Lett. **110**, 055702 (2013)

66. J. Dzubiella, G.P. Hoffmann, H. Löwen, Phys. Rev. E **65**, 021402 (2002)
67. T. Vissers, A. Wysocki, M. Rex, H. Löwen, C.P. Royall, A. Imhof, A. van Blaaderen, Soft Matter **7**, 2352 (2011)
68. J. Dunkel, S. Heidenreich, K. Drescher, H.H. Wensink, M. Bär, R.E. Goldstein, Phys. Rev. Lett. **110**, 228102 (2013)
69. L. Giomi, Phys. Rev. X **5**, 031003 (2015)
70. R. Grossmann, P. Romanczuk, M. Bär, L. Schimansky-Geier, Phys. Rev. Lett. **113**, 258104 (2014)
71. J.M. Yeomans, Nat. Mater. **13**, 1004 (2014)
72. V. Bratanov, F. Jenko, E. Frey, PNAS **112**, 15048 (2015)
73. A. Kaiser, A. Peshkow, A. Sokolov, B. ten Hagen, H. Löwen, I.S. Aranson, Phys. Rev. Lett. **112**, 158101 (2014)
74. A. Kaiser, A. Sokolov, I.S. Aranson, H. Löwen, Eur. Phys. J. Special Topics **224**, 1275 (2015)
75. M. Marechal, R.J. Kortschot, A.F. Demirörs, A. Imhof, M. Dijkstra, Nano Lett. **10**, 1907 (2010)
76. K.-A. Liu, L. I, Phys. Rev. E **86**, 011924 (2012)
77. Y.-S. Su, H.-C. Wang, L. I, Phys. Rev. E **91**, 030302(R) (2015)
78. H. Wioland, F.G. Woodhouse, J. Dunkel, R.E. Goldstein, Nat. Phys. **12**, 341 (2016)
79. A. Kaiser, H. Löwen, Phys. Rev. E **87**, 032712 (2013)
80. Y. Yang, F. Qiu, G. Gompper, Phys. Rev. E **89**, 012720 (2014)
81. R. Sknepnek, S. Henkes, Phys. Rev. E **91**, 022306 (2015)